iScience

CellPress
OPEN ACCESS

Article

Fusobacterium nucleatum promotes colorectal cancer metastasis by excretion of miR-122-5p from cells via exosomes

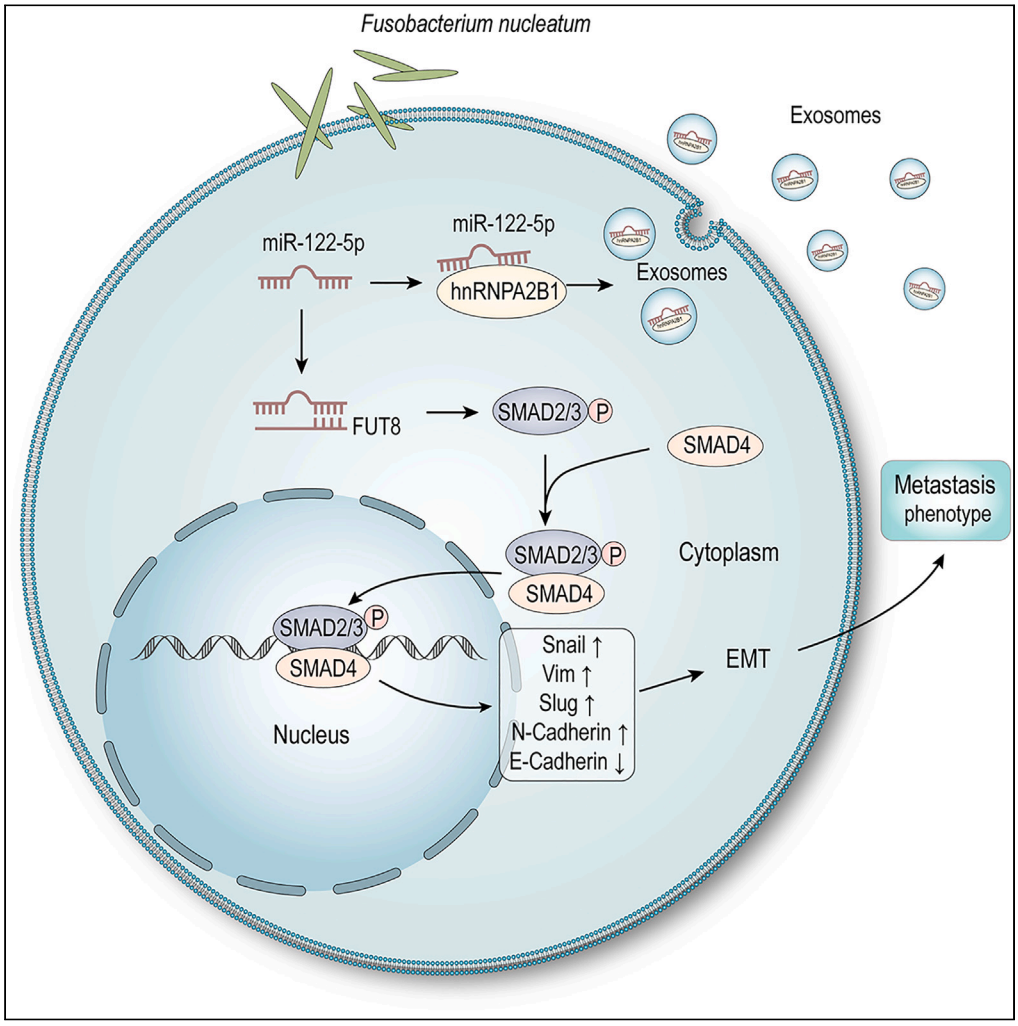

Mengjiao Zhang, Yifeng Wang, Longchen Yu, ..., Nannan Ning, Yi Zhang, Xin Zhang

yizhang@sdu.edu.cn (Y.Z.)
xinzhang@sdu.edu.cn (X.Z.)

Highlights

Fusobacterium nucleatum infection enhances exosomal miR-122-5p level

Fusobacterium nucleatum infection decreases intracellular miR-122-5p expression

Secretion of miR-122-5p into exosomes is mediated by hnRNPA2B1

FUT8 is the target gene of miR-122-5p

Zhang et al., iScience 26, 107686
September 15, 2023
https://doi.org/10.1016/j.isci.2023.107686

iScience

CellPress
OPEN ACCESS

Article

Fusobacterium nucleatum promotes colorectal cancer metastasis by excretion of miR-122-5p from cells via exosomes

Mengjiao Zhang,[1,2,5] Yifeng Wang,[1,2,5] Longchen Yu,[1,2] Yanli Zhang,[3] Yanlei Wang,[4] Ziqi Shang,[1,2] Yiwei Xin,[1,2] Xinyang Li,[1,2] Nannan Ning,[1,2] Yi Zhang,[1,2,*] and Xin Zhang[1,2,6,*]

SUMMARY

***Fusobacterium nucleatum (Fn)* infection and microRNAs (miRNAs) are closely associated with colorectal cancer (CRC) development, but the mechanism by which *Fn* regulates tumor-suppressive miRNAs via exosomes and facilitates CRC metastasis remains unclear. Here, we identified that *Fn* infection significantly increased exosomal miR-122-5p levels in the serum of CRC patients and CRC cell culture supernatants through two miRNA panels of high-throughput sequencing and RT-qPCR analysis. In *Fn*-infected patients, the serum exosomal levels of miR-122-5p were negatively associated with their expression levels of tissues. Downregulated miR-122-5p was demonstrated to enhance the migration, invasion, and metastasis abilities of CRC cells *in vivo* and *in vitro*. Secretion of miR-122-5p into exosomes is mediated by hnRNPA2B1. Mechanistically, *Fn* activated the TGF-β1/Smads signaling pathway to promote EMT by regulation of the miR-122-5p/FUT8 axis. In conclusion, *Fn* infection may stimulate CRC cells to excrete exosome-wrapped miR-122-5p, and activate the FUT8/TGF-β1/Smads axis to promote metastasis.**

INTRODUCTION

Colorectal cancer (CRC) ranks third in incidence and second in mortality among all malignant tumors.[1] Despite improvements in screening and treatment approaches, CRC still has a poor 5-year survival rate due to metastasis.[2] Metastasis is a multistep and complex process regulated by a multigenic system that worsens CRC outcomes.[3,4] Thus, it is urgently necessary to explore the mechanisms underlying CRC metastasis and facilitate the identification of effective therapeutic strategies to prevent metastasis and improve the prognosis of CRC patients.

Mounting evidence has been reported that the gut microbiota plays an important role in CRC development and progression.[5,6] In particular, *Fusobacterium nucleatum* (*Fn*), a gram-negative obligate anaerobic bacterium, is enriched in colorectal carcinomas and contributes to CRC pathogenesis.[7–9] Moreover, *Fn* is predominantly associated with metastatic tumor cells from primary CRC.[10] Our previous study revealed a potential link between *Fn* abundance and CRC metastasis and suggested that *Fn* is a risk factor for metastatic CRC.[11] Recent studies have reported that *Fn* enhances the migratory and invasive activities of CRC cells by increasing the expression of some noncoding RNAs, such as microRNA-21,[12] long noncoding RNA EVADR,[13] and keratin-7 antisense.[14] However, little research has been performed to investigate the mechanism by which *Fn* regulates tumor suppressors and facilitates CRC metastasis.

As a tumor suppressor gene, miR-122-5p has been reported to inhibit the proliferation, migration, and invasion of cancer cells.[15–17] For example, miR-122 functions as a tumor suppressor and plays a vital role in inhibiting the progression of breast cancer through targeting IGF1R and regulating PI3K/Akt/mTOR/p70S6K pathway.[15] miR-122-5p knockdown partially reversed SNHG7 silencing-induced tumor-suppressive effects on hepatocellular carcinoma cells.[18] Moreover, it had been reported that miR-122-5p expression was downregulated in intrahepatic cholangiocarcinoma (iCCA) tissues, regulated FUT8 expression in iCCA cells, and inhibited FUT8-induced cell migration and proliferation through PI3K/AKT signaling pathway.[19] However, the molecular mechanism involved in the role of miR-122-5p in CRC remains unclear.

Exosomes are membrane microvesicles (30–100 nm in size) that are secreted by cells or shed from the cell membrane.[20] Recent report has revealed that exosomes from *Fn*-infected CRC cells increase their tumor metastatic capability by transferring miR-1246/92b-3p/27a-3p into neighboring noninfected cancer cells.[21] Nevertheless, the majority of reports regarding exosomal miRNAs have focused on oncogenic-related molecules in cancer cells. Indeed, exosome cargoes have been reported to contain numerous tumor-suppressive RNAs.[22] Thus, it is necessary to explore whether tumor cells excrete suppressive miRNAs via exosomes to facilitate escape from antitumor processes.

[1]Department of Clinical Laboratory, Qilu Hospital of Shandong University, Jinan 250012, China
[2]Shandong Engineering Research Center of Biomarker and Artificial Intelligence Application, Jinan 250012, China
[3]Department of Clinical Laboratory, Shandong Provincial Third Hospital, Jinan 250031, China
[4]Department of General Surgery, Qilu Hospital of Shandong University, Jinan 250012, China
[5]These authors contributed equally
[6]Lead contact
*Correspondence: yizhang@sdu.edu.cn (Y.Z.), xinzhang@sdu.edu.cn (X.Z.)
https://doi.org/10.1016/j.isci.2023.107686

In this study, we attempted to use exosomal miRNAs to determine the association between *Fn* infection and CRC metastasis and the underlying mechanisms. We identified that *Fn* facilitated tumor metastasis by promoting the excretion of tumor-suppressive miR-122-5p from colorectal cells via exosomes. Mechanistically, selective downregulation of miR-122-5p in CRC cells resulted in reduced intracellular inhibition of FUT8 and activation of the TGF-β1/Smads prometastasis signaling pathway. Our data provide evidence that *Fn* and miRNAs wrapped in exosomes could serve as potential therapeutic targets for the treatment of CRC.

RESULTS

miR-122-5p is enriched in exosomes secreted by *Fn*-infected CRC cells

To identify potential exosomal miRNAs involved in *Fn* infection, we first compared two panels of exosomal miRNA expression profiles by miRNA sequencing. These two panels included exosomes isolated from the serum of CRC patients with distinct *Fn* abundance (GSE215093) and exosomes derived from CRC cells treated with *Fn* or PBS (GSE216142). The characteristics of exosomes were confirmed by transmission electron microscopy, nanoparticle tracking system, and western blotting for the exosome markers CD63, Alix, and TSG101 and the absence of the endoplasmic reticulum marker calnexin in exosomes (Figures S1A–S1C). As shown in Figure 1A, 183 upregulated and 193 downregulated miRNAs were identified in the serum exosomes of CRC patients with a high abundance of *Fn* (|fold change| >2 and $p < 0.05$). Simultaneously, 155 upregulated and 45 downregulated miRNAs were identified in the exosomes of *Fn*-infected CRC cells (|fold change| >2 and $p < 0.05$) (Figure 1B). After taking the intersection, miR-122-5p was identified as the most prominently upregulated miRNA in both panels. To verify the previously described miRNA sequencing findings, 5 CRC cell lines (LOVO, HCT116, SW620, SW480, and HT29) were co-cultured with PBS, *E. coli*, *Fn49256*, or *Fn25586*. As expected, treatment with *Fn49256* and *Fn25586* infection significantly increased the levels of exosomal miR-122-5p (Figure 1C).

To further illuminate whether miR-122-5p was mainly derived from the exosomes of CRC cells, GW4869, a well-known exosome inhibitor, was used to block exosome secretion. As expected, we identified that the levels of miR-122-5p in CM of CRC cells were dramatically reduced following GW4869 treatment (Figure 1D). CRC cell-derived exosomes were treated with RNase A, an enzyme that can degrade RNAs. Results showed that miR-122-5p expression was unchanged (Figure 1E). Next, we employed Triton X-100, an agent usually used to increase membrane permeability, to treat exosomes and we found RNase A decreased miR-122-5p expression (Figure 1E). These data indicated that extracellular miR-122-5p was packaged into membranes instead of exuding outside of the tumor cells directly. Subsequently, we observed that miR-122-5p was predominantly localized in the cytoplasm of SW480 and HCT116 cells (Figure 1F), which was further corroborated by the fluorescence *in situ* hybridization assay (Figure 1G). These results suggest that miR-122-5p may exert its biological function in the cytoplasm.

Thus, these data collectively reveal that miR-122-5p is enriched in *Fn*-infected CRC cell-derived exosomes.

Fn infection is associated with miR-122-5p expression in CRC patients

To investigate the relationship between *Fn* infection and miR-122-5p expression, we enrolled 30 CRC patients with *Fn* infection and 30 CRC patients without *Fn* infection. Data from Figure 2A revealed that miR-122-5p levels in *Fn*-positive CRC tissues were lower than those in *Fn*-negative tissues. Compared with corresponding non-tumor normal tissues, miR-122-5p downregulation rate reached 73.3% (22/30) in *Fn*-positive tissues, while there was only 40% (12/30) in *Fn*-negative tissues (Figure 2B). Meanwhile, miR-122-5p expression was significantly higher in exosomes of serum from *Fn*-positive CRC patients than that in *Fn*-negative patients (Figure 2C). In *Fn*-positive groups, there was a significantly negative correlation between the expression of miR-122-5p in circulating serum and tissues, whose correlation was better than that in *Fn*-negative cohort (Figure 2D). In addition, exosomal miR-122-5p was significantly increased in the serum of 60 CRC patients compared with healthy controls (Figure S2A). These data were validated using external GEO cohorts (GSE106817, GSE112264, GSE113486, and GSE124158) (Figure S2B). Of note, the upregulation of exosomal miR-122-5p was positively associated with lymph node metastasis and distal metastasis status but not with other clinicopathologic characteristics (Table S1). Overall, we speculate that *Fn*-mediated tumor promotion partly depends on intracellular miR-122-5p being released into exosomes.

Decreased miR-122-5p caused by *Fn* infection promotes CRC metastasis

To understand how miR-122-5p exerts its effects in *Fn*-infected CRC cells, we measured the intracellular miR-122-5p expression levels after *Fn* treatment. As expected, *Fn* infection resulted in the downregulation of miR-122-5p expression in CRC cells (Figure 3A). Due to the association between miR-122-5p expression and tumor metastasis demonstrated in clinical samples, we performed *in vitro* and *in vivo* experiments to explore whether miR-122-5p had a marked effect on CRC metastasis. miRNA mimics, which are synthesized using chemical synthesis methods, are mimics of endogenous miRNAs in organisms and can enhance the function of endogenous miRNAs. miRNA inhibitor is chemically modified single-stranded oligonucleotides that specifically targets and inhibits the function of endogenous miRNAs. When transfected with miR-122-5p mimics, transwell and wound healing assays showed that the migration and invasion of SW480 cells were significantly inhibited, while the opposite phenomena were observed when miR-122-5p was inhibited (Figures 3B–3D). Simultaneously, results revealed that *Fn* could facilitate the migration and invasion of SW480 cells (Figures 3B–3D). Nevertheless, the pro-tumor activity triggered by *Fn* infection was significantly blocked by overexpression of miR-122-5p (Figures 3B–3D). Similar results were observed in HCT116 cells (Figures S3A–S3C).

Next, we established the CRC metastasis mouse model via intrasplenic injection. Compared with PBS treatment or miR-NC treatment, *Fn* infection increased liver metastatic growth, whereas overexpression of miR-122-5p markedly reduced the metastatic hepatic nodules

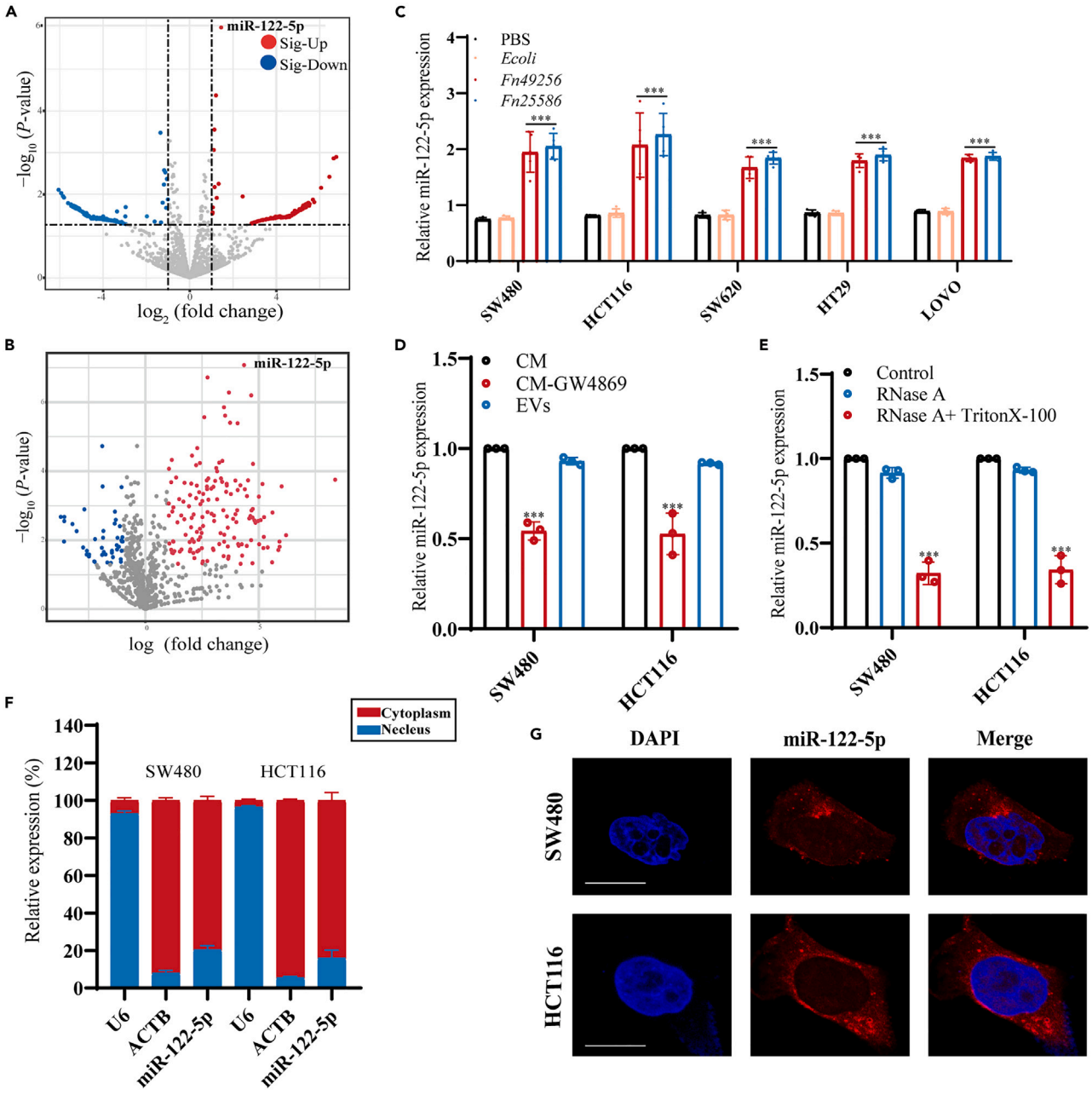

Figure 1. miR-122-5p is enriched in exosomes secreted by *Fn*-infected CRC cells

(A) Volcano map of differentially miRNA expressed genes in serum exosomes of CRC patients with high or low *Fn* abundance. Red denotes upregulation; green denotes downregulation.

(B) Volcano map showing the significantly differentially expressed miRNAs in *Fn*-infected and uninfected SW480 cell-derived exosomes. Red denotes upregulation; green denotes downregulation.

(C) Exosomal miR-122-5p expression in 5 CRC cells (SW480, HCT116, SW620, HT29, LOVO) treated with PBS, *E. coli*, *Fn49256*, or *Fn25586* confirmed by RT-qPCR. Data represent mean ± SEM.

(D) The culture medium was added with or without GW4869. Quantitative analysis of miR-122-5p expression in the CM or exosomes of HCT116 and SW480 cells. (Conditioned medium, CM). Data represent mean ± SEM.

(E) miR-122-5p expression in HCT116 and SW480-derived exosomes treated with RNase A alone or together with Triton X-100. Data represent mean ± SEM.

(F) The levels of miR-122-5p in the nuclear and cytoplasmic portions of HCT116 and SW480 cells. Data represent mean ± SEM.

(G) Fluorescence *in situ* hybridization (FISH) detection of miR-122-5p in CRC cells. miR-122-5p was stained with probe (red) and nuclei were stained with DAPI (blue). Scale bar, 10 μm. *p < 0.05, **p < 0.01, ***p < 0.001.

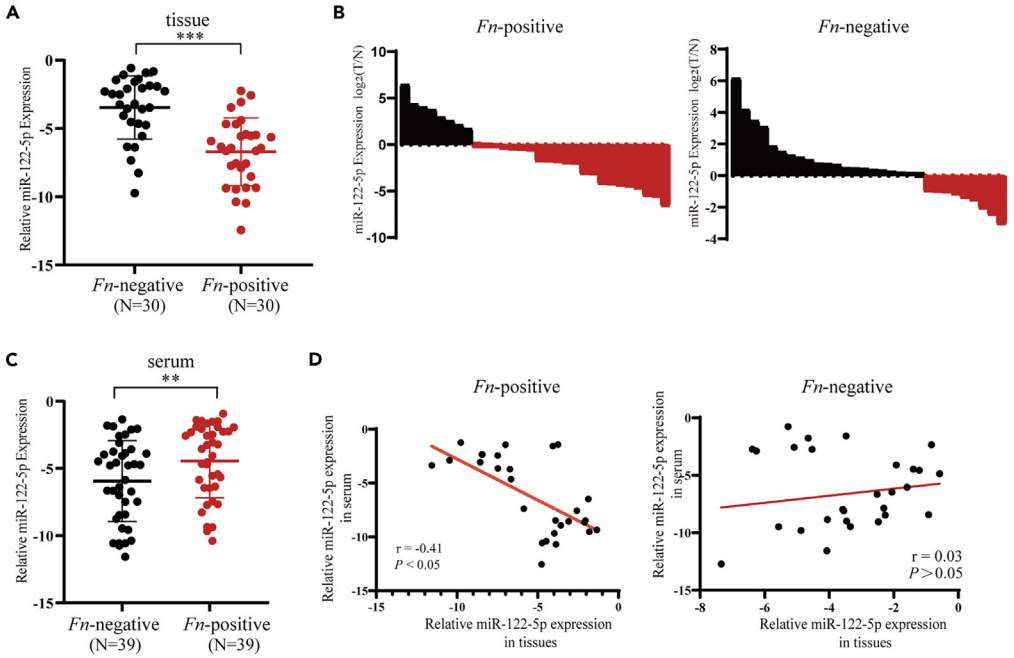

Figure 2. *Fn* abundance is associated with miR-122-5p expression in CRC patients

(A) Relative levels of miR-122-5p in CRC tissues with and without *Fn* infection, each group 30 samples. Data represent mean ± SEM.

(B) miR-122-5p downregulation rate in *Fn*-positive and *Fn*-negative tissues. Data represent mean ± SEM.

(C) miR-122-5p expression in *Fn*-positive and *Fn*-negative serum. Data represent mean ± SEM.

(D) The correlation of miR-122-5p expression between CRC tissues and circulating serum in *Fn*-positive CRC patients (r = −0.41, p < 0.05) and those in *Fn*-negative CRC patients (r = 0.03, p >0.05). *p < 0.05, **p < 0.01, ***p < 0.001.

subsequent to *Fn* infection. H&E staining further revealed the morphology of liver metastases (Figure 3E). Taken together, these data suggest that *Fn* could decrease suppressive miR-122-5p expression and promote tumor metastasis.

Secretion of miR-122-5p into exosomes is mediated by hnRNPA2B1

To explore how intracellular miR-122-5p is delivered into exosomes, we initially structured a hostile environment that was not conducive to the growth of tumor cells by overexpressing tumor-suppressive miR-122-5p. Results showed that the expression of miR-122-5p in exosome-derived tumor cells overexpressing miR-122-5p was dramatically enhanced compared to that in the untreated group (Figure 4A). Recent studies have reported that RNA-binding proteins mediate the specific sorting of miRNAs into exosomes.[23] We observed that hnRNPA2B1, which is considered an RNA-binding protein, contained specific GGAG motifs that enable it to bind to miR-122-5p and control the loading of miR-122-5p into exosomes. RNA pull-down assays demonstrated that hnRNA2B1 could bind miR-122-5p WT but not miR-122-5p MUT (Figure 4B). RNA immunoprecipitation assays further confirmed that miR-122-5p was more enriched in the anti-hnRNPA2B1 antibody group than in the anti-IgG group (Figure 4C). Interestingly, *Fn* treatment resulted in increased hnRNPA2B1 levels, which suggests that *Fn* accelerated CRC metastasis by promoting secretion of the suppressive miR-122-5p into exosomes (Figure 4D).

To clarify whether the *Fn*-induced packaging of miR-122-5p into exosomes was dependent on hnRNPA2B1, we designed siRNAs for hnRNPA2B1, and the knockdown efficiency was validated by RT-qPCR and western blotting (Figure 4E). Knockdown of hnRNPA2B1 resulted in significantly increased intracellular miR-122-5p levels and a reduced exo/cell miR-122-5p ratio (Figure 4F). In further analysis, we observed that si-hnRNPA2B1 repressed the migration and invasion of *Fn*-infected CRC cells; this could be partly reversed by miR-122-5p inhibitors (Figures 4G and S5A). Thus, we hypothesize that *Fn* could drive intracellular miR-122-5p to leave cells and be packaged into exosomes. This secretion of miR-122-5p into exosomes may be mediated by hnRNPA2B1.

FUT8 is the target gene of miR-122-5p in *Fn*-infected CRC cells

To elucidate the underlying molecular mechanism by which miR-122-5p exerts its effects in *Fn*-infected CRC cells, we investigated its target mRNA in CRC tissues with differential abundances of *Fn* (SRA: PRJNA777960). Among the upregulated genes in CRC tissues with highly enriched *Fn* (Table S2), 6 genes contained binding sites for miR-122-5p as per starBase prediction (Figure 5A; Table S3). Further analysis indicated that only FUT8 had an enhanced level in *Fn*-infected CRC cells compared with uninfected cells (Figure S6A). It was predicted that a targeting region of the FUT8 3′UTR bound to hsa-miR-122-5p at position 460–466. To verify this prediction, FUT8 3′UTR-binding sites

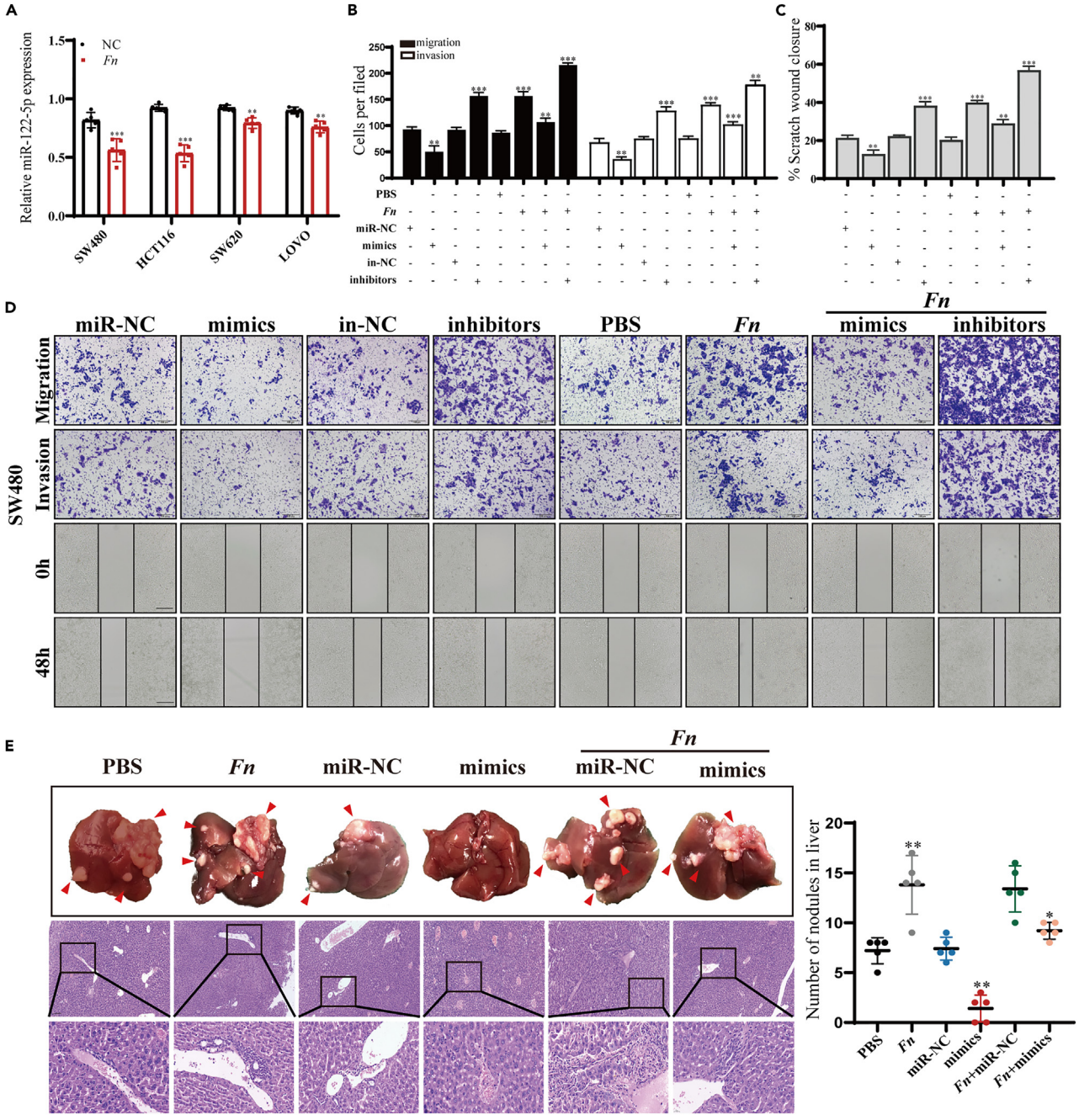

Figure 3. Decreased miR-122-5p in CRC cells induced by *Fn* promotes tumor metastasis

(A) Expression of miR-122-5p in FHC, SW480, and HCT116 cells following *Fn* infection. Data represent mean ± SEM.

(B and C) Histogram analysis of transwell and wound healing assays. Data represent mean ± SEM.

(D) Transwell and wound healing assays were performed to value the migratory and invasive abilities of SW480 cells transfected with miR-122-5p mimics, inhibitors or treated with PBS, *Fn*. Scale bar, 100 μm.

(E) Left: Representative gross and H&E images of CRC liver in mice from the indicated group. Scale bar, 100 μm. Right: The quantification of the liver metastatic foci. Data represent mean ± SEM. *p < 0.05, **p < 0.01, ***p < 0.001.

containing wild-type or mutated sequences were inserted into luciferase reporter vectors. The results demonstrated that miR-122-5p overexpression strikingly suppressed FUT8 luciferase activity, while this effect was completely abolished in *Fn*-infected CRC cells transfected with the mutated vector (Figures 5B and S6B). Western blotting and RT-qPCR assays demonstrated that miR-122-5p overexpression lowered

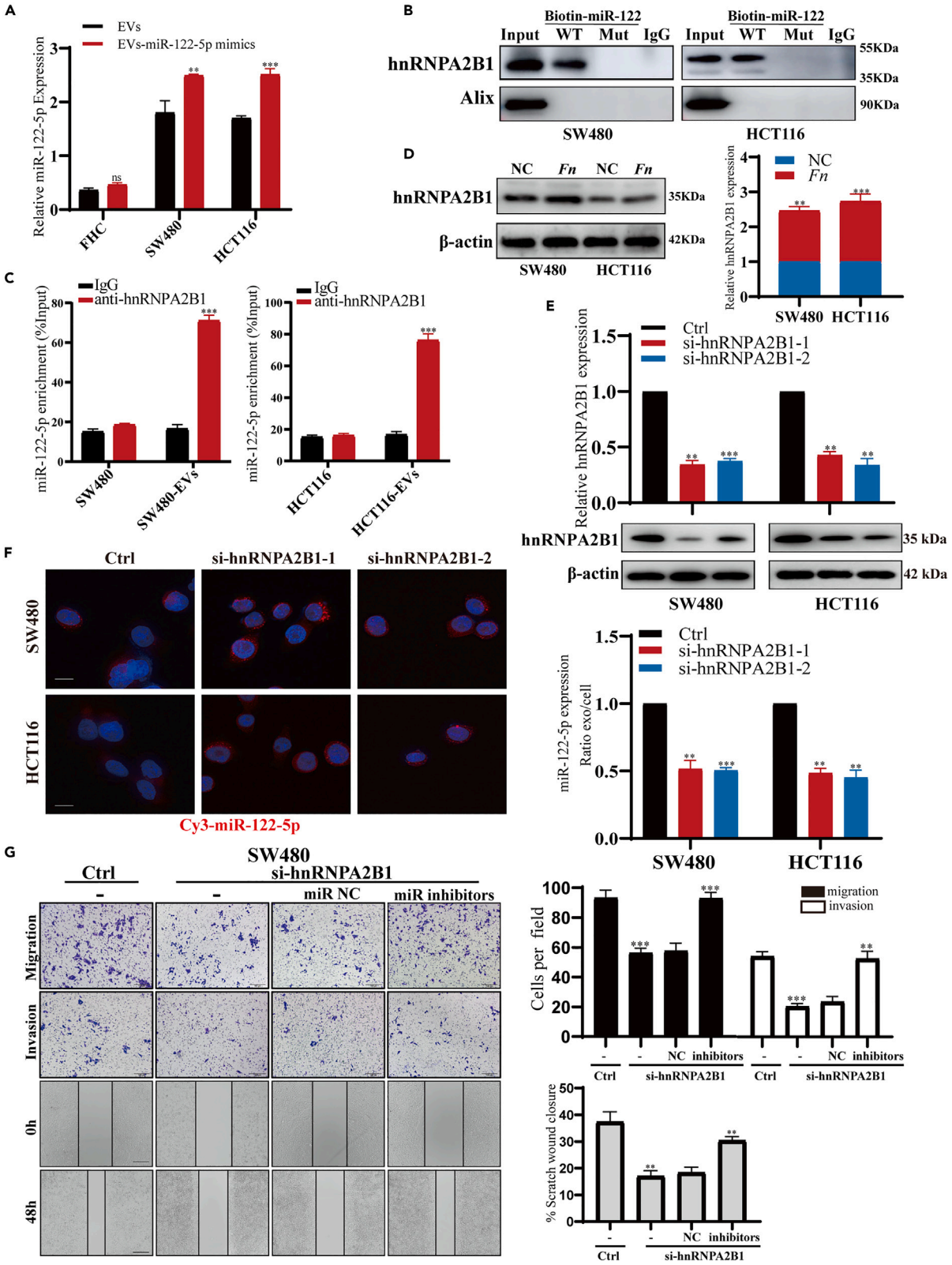
A
EVs
EVs-miR-122-5p mimics
Relative miR-122-5p Expression
ns
FHC
SW480
HCT116
B
Biotin-miR-122
Input WT Mut IgG
Input WT Mut IgG
hnRNPA2B1
Alix
55KDa
35KDa
90KDa
SW480
HCT116
C
IgG
anti-hnRNPA2B1
miR-122-5p enrichment (%Input)
SW480
SW480-EVs
HCT116
HCT116-EVs
D
NC Fn NC Fn
hnRNPA2B1
β-actin
35KDa
42KDa
SW480 HCT116
NC
Fn
Relative hnRNPA2B1 expression
SW480 HCT116
E
Ctrl
si-hnRNPA2B1-1
si-hnRNPA2B1-2
Relative hnRNPA2B1 expression
hnRNPA2B1
β-actin
35 kDa
42 kDa
SW480
HCT116
Ctrl
si-hnRNPA2B1-1
si-hnRNPA2B1-2
miR-122-5p expression
Ratio exo/cell
SW480
HCT116
F
Ctrl
si-hnRNPA2B1-1
si-hnRNPA2B1-2
SW480
HCT116
Cy3-miR-122-5p
G
SW480
Ctrl
si-hnRNPA2B1
-
-
miR NC
miR inhibitors
Migration
Invasion
0h
48h
migration
invasion
Cells per field
- - NC inhibitors - - NC inhibitors
Ctrl
si-hnRNPA2B1
Ctrl
si-hnRNPA2B1
% Scratch wound closure
- - NC inhibitors
Ctrl
si-hnRNPA2B1

Figure 4. Secretion of miR-122-5p into exosomes is mediated by hnRNPA2B1

(A) Quantitative analysis of exosomal miR-122-5p expression when overexpressed miR-122-5p in cells. Data represent mean ± SEM.

(B) RNA pull-down assay was performed to determine that wild-type miR-122-5p bound to hnRNPA2B1, yet this binding strength was weakened when mutating miR-122-5p in exosomes.

(C) RIP was performed with anti-hnRNPA2B1 antibody on exosomes derived from SW480/HCT116-CM to assess hnRNPA2B1 binding to miR-122-5p and RNA extracted from the immunoprecipitation was used to analyze the expression of miR-122-5p. Percentage of miR-122-5p was relative to the input sample (% input). IgG regarded as negative control. Data represent mean ± SEM.

(D) hnRNPA2B1 expression was detected by western blotting in CRC cells with or without *Fn* infection.

(E) RT-qPCR and Western blotting results showed the knockdown efficiency of hnRNPA2B1 siRNAs. Data represent mean ± SEM.

(F) Left: Representative fluorescent images of Cy3-labled miR-122-5p in SW480 and HCT116 cells transfected with hnRNPA2B1 siRNA or NC siRNA. Right: Quantitative analysis of the exo/cell ratio of miR-122-5p expression in above treatment groups. Scale bar, 10 μm. Data represent mean ± SEM.

(G) Transwell assays and wound healing assays indicated that the inhibitory migratory and invasive effect of hnRNPA2B1 knockdown in SW480 cells could be reversed by miR-122-5p inhibitor. Scale bar, 100 μm. Data represent mean ± SEM. *p < 0.05, **p < 0.01, ***p < 0.001.

FUT8 expression both at the protein and mRNA levels. Moreover, the miR-122-5p-induced downregulation of FUT8 was rescued by reintroduction of FUT8, and upregulation of FUT8 by miR-122-5p inhibitors was partially reversed by silencing FUT8 (Figures 5C and S6C). Furthermore, we detected FUT8 expression in colorectal tissues, and as expected, the expression of FUT8 was higher in CRC tissues than in adjacent normal tissues (Figure 5D). Meanwhile, a negative correlation between miR-122-5p and FUT8 levels was also observed in CRC tissues (Figure 5E). The FUT8 expression patterns and the previously described correlation were further confirmed in TCGA databases (Figures S6D and S6E).

Besides, we also detected a higher level of FUT8 in CRC tissues with high *Fn* abundance than in those with low *Fn* abundance by immunohistochemistry (Figure 5F). To ascertain whether FUT8 was the downstream regulator of *Fn*-induced CRC metastasis, western blotting and RT-qPCR were applied to detect FUT8 expression in CRC cells following *Fn* treatment. Results revealed that *Fn* infection enhanced the expression of FUT8, which could be abolished by overexpression of miR-122-5p. Meanwhile, miR-122-5p inhibition increased the upregulation of FUT8 induced by *Fn* stimulation (Figures 5G and S6F). Furthermore, in *in vivo* experiments, we observed that sh-FUT8 successfully restrained tumor metastasis induced by *Fn* (Figure 5H).

Collectively, these findings indicated that FUT8 was a downstream target of miR-122-5p and contributed to the mechanisms of CRC.

The *Fn*/miR-122-5p/FUT8 axis promotes EMT via activation of the TGF-β1/Smads signaling pathway

We verified the mechanisms by which the miR-122-5p/FUT8 axis functions in *Fn*-induced CRC metastasis. Figure 6A reveals that FUT8-overexpressing CRC cells displayed morphological conversion into a mesenchymal phenotype. Furthermore, altered phenotypes were accompanied by reduced mRNA and protein levels of E-cadherin but increased N-cadherin, Vimentin, Snail, and Twist levels, while sh-FUT8 treatment resulted in the opposite effect. Results further showed that FUT8-induced epithelial-mesenchymal transition (EMT) could be reversed by miR-122-5p overexpression (Figures 6B, S8A, and S8B). To pinpoint the in-depth mechanism by which FUT8 functions to cause EMT, we induced EMT in SW480 and HCT116 cells using TGF-β1, which is considered to be a potent regulator of EMT and was shown to induce tumor metastasis via the TGF-β1/Smads signaling pathway.[24] Following TGF-β1 treatment, markers of EMT initiation were observed by western blotting, but this enhanced process was significantly reversed by knockout of FUT8 (Figure S8C). Moreover, we observed that FUT8 expression was elevated upon TGF-β1 stimulation, whereas weakened effects were observed when miR-122-5p was overexpressed (Figure 6C). Besides, we further noted a positive correlation between the expression of TGF-β1 and FUT8 in CRC tissues (Figure 6D). Thus, it was reasonable to speculate that the *Fn*/miR-122-5p/FUT8 axis facilitated EMT by activating the TGF-β1 signaling pathway.

Next, the downstream molecules of the TGF-β1 signaling pathway were detected. As expected, miR-122-5p inhibition elevated the phosphorylation levels of Smad2 and Smad3 and activated the TGF-β1/Smads signaling pathway (Figures 6E and S8D). To further validate whether miR-122-5p regulated EMT in a TGF-β1/Smads signaling pathway-dependent manner, we applied SB431542 to inhibit Smad2/3 phosphorylation. Results confirmed that SB431542 repressed the EMT status induced by miR-122-5p inhibition, a process that was reversed by the introduction of FUT8 (Figures 6F and S8D). Furthermore, suppression of Smad2/3 phosphorylation by SB431542 additionally blocked FUT8 protein expression. To further investigate whether *Fn*-induced TGF-β1/Smads pathway activation was involved in the regulation of FUT8, SB431542 was used to treat *Fn*-infected CRC cells. Results revealed that the upregulated levels of FUT8 induced by *Fn* infection were obviously attenuated by SB431542 (Figures 6G and S8E). Consistently, SB431542 treatment weakened the migration and invasion levels of CRC cells after *Fn* treatment (Figures 6H and S8F).

Overall, our studies suggested that *Fn* activated the TGF-β1/Smads signaling pathway to promote EMT by regulating the miR-122-5p/FUT8 axis.

DISCUSSION

At present, it is known that *Fn* infection is closely related to the CRC occurrence and development. Currently, multiple studies have reported that *Fn* infection can increase the expression of some oncogenic miRNAs to sustain CRC cell viability.[12,25] However, little is known about the effects of *Fn* on oncosuppression in CRC. This study is the first to demonstrate that decreased levels of miR-122-5p promote EMT through activation of the FUT8/TGF-β1/Smads axis in *Fn*-infected CRC cells. And, *Fn* facilitates CRC metastasis by downregulating intracellular

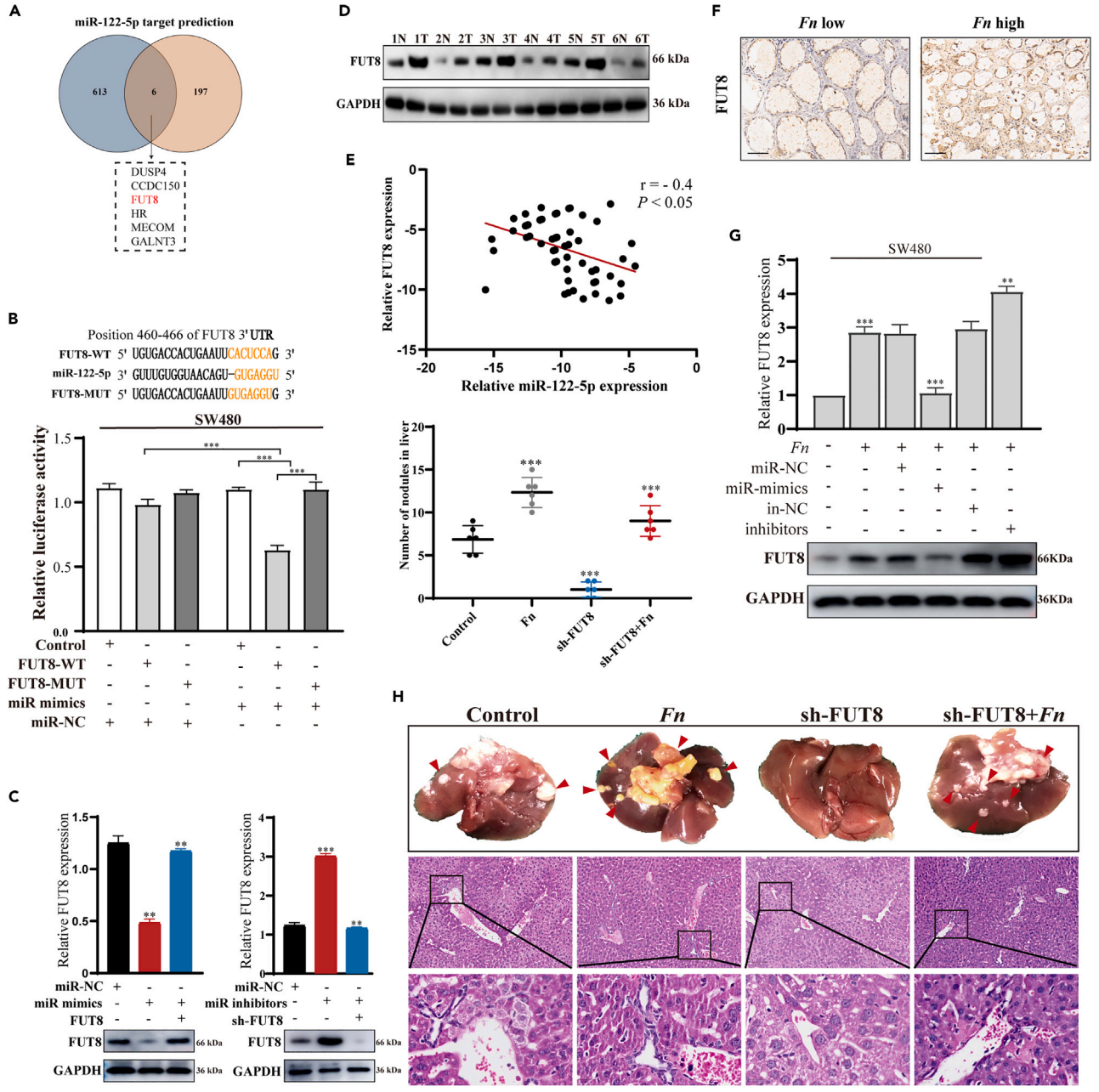

Figure 5. miR-122-5p directly targets FUT8 expression in *Fn*-infected CRC cells

(A) Overlap analysis to detect the target gene of miR-122-5p. Left: increased mRNAs from CRC tissues with highly enriched Fn (SRA: PRJNA777960). Right: predicted target genes of miR-122-5p from starBase database.

(B) The luciferase reporter experiment was applied to target sequences of the 3′-UTR of FUT8 by miR-122-5p. Data represent mean ± SEM.

(C) Relative FUT8 expression in *Fn*-infected SW480 cells following miR-122-5p mimics or miR-122-5p inhibitors. Data represent mean ± SEM.

(D) Western blotting results showed FUT8 expression in 6 pairs cancer tissue and matched normal colon mucosa.

(E) Correlation of miR-122-5p and FUT8 expression in CRC tissues (r = −0.3975, p < 0.05).

(F) IHC staining assay showed that FUT8 expression in CRC tissues with low or high *Fn* enrichment. Scale bar, 100 μm.

(G) Expression levels of FUT8 in SW480 cells treated with *Fn* alone or together transfected with miR-122-5p mimics or miR-122-5p inhibitors. Data represent mean ± SEM.

(H) Representative gross and H&E images of CRC liver metastases in mice and the quantification of the liver metastatic foci. Scale bar, 100 μm. Data represent mean ± SEM. *p < 0.05, **p < 0.01, ***p < 0.001.

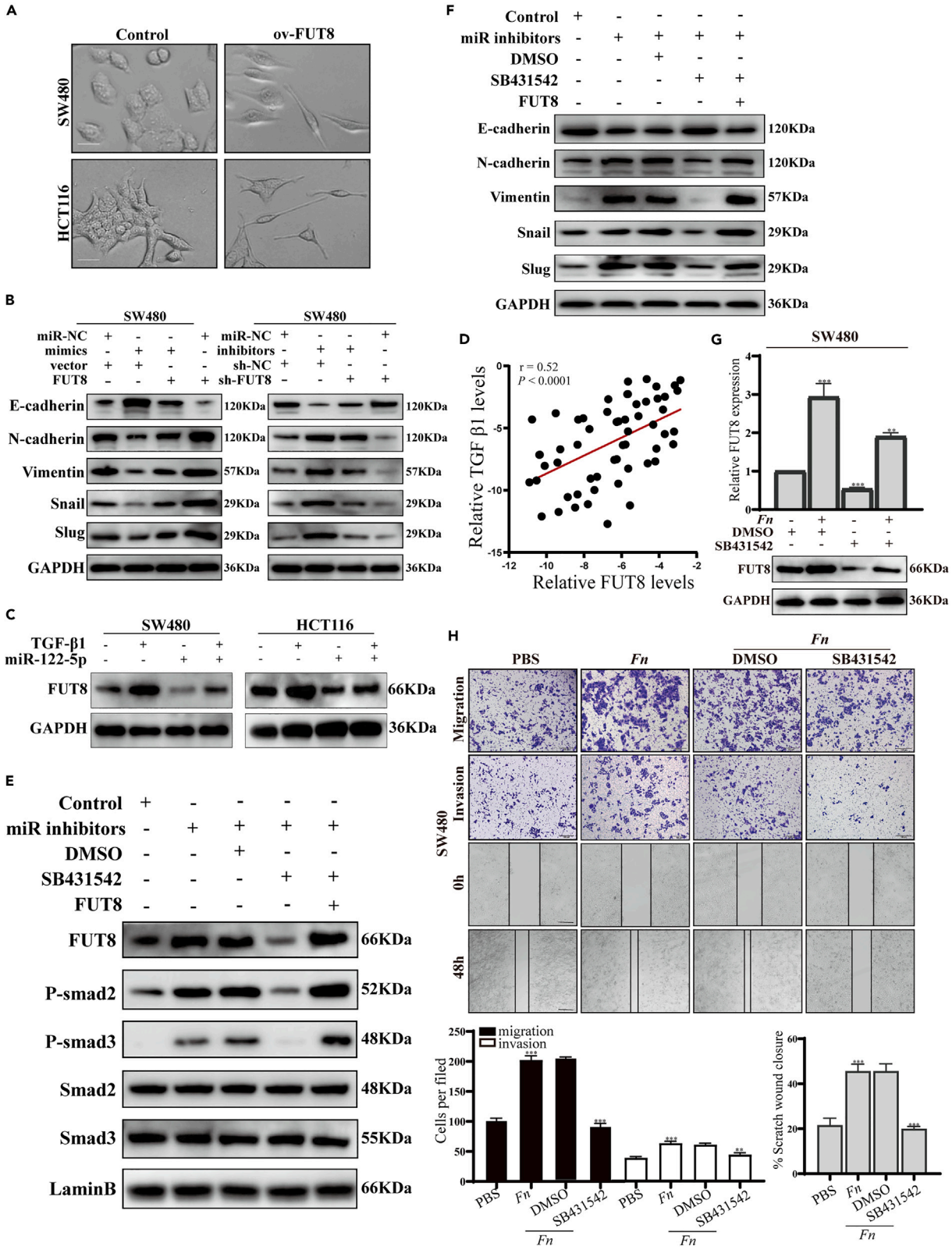
A
Control
ov-FUT8
SW480
HCT116
B
SW480
SW480
miR-NC
mimics
vector
FUT8
miR-NC
inhibitors
sh-NC
sh-FUT8
E-cadherin
N-cadherin
Vimentin
Snail
Slug
GAPDH
120KDa
57KDa
29KDa
36KDa
C
SW480
HCT116
TGF-β1
miR-122-5p
FUT8
GAPDH
66KDa
36KDa
D
r = 0.52
P < 0.0001
Relative TGF β1 levels
Relative FUT8 levels
E
Control
miR inhibitors
DMSO
SB431542
FUT8
FUT8
P-smad2
P-smad3
Smad2
Smad3
LaminB
66KDa
52KDa
48KDa
48KDa
55KDa
66KDa
F
Control
miR inhibitors
DMSO
SB431542
FUT8
E-cadherin
N-cadherin
Vimentin
Snail
Slug
GAPDH
120KDa
120KDa
57KDa
29KDa
29KDa
36KDa
G
SW480
Relative FUT8 expression
Fn
DMSO
SB431542
FUT8
GAPDH
66KDa
36KDa
H
PBS
Fn
DMSO
SB431542
Fn
Migration
Invasion
SW480
0h
48h
migration
invasion
Cells per filed
% Scratch wound closure
PBS
Fn
DMSO
SB431542
Fn

Figure 6. The *Fn*/miR-122-5p/FUT8 axis promotes EMT via activation of the TGF-β1/Smads signaling pathway to facilitate CRC metastasis

(A) FUT8 overexpression in CRC cells induced morphological alterations similar to EMT. Scale bar, 10 μm.

(B) EMT markers were determined by Western blotting in SW480 cells transfected with miR-122-5p or FUT8.

(C) FUT8 expression levels in CRC cells treated with TGF-β1, miR-122-5p mimics, or together with TGF-β1 and miR-122-5p mimics.

(D) FUT8 expression was positively correlated with TGF-β1 expression in CRC tissues ($r = -0.5215$, $p < 0.0001$).

(E) Western blotting of SMAD2/3, *p*-SMAD2/3, and FUT8 protein levels in different groups.

(F) EMT markers were detected by Western blotting in SW480 cells.

(G) SW480 cells were incubated with *Fn* alone or together with SB431542. FUT8 protein was analyzed by Western blotting. Data represent mean ± SEM.

(H) SW480 cells treated with SB431542 were co-cultured with *Fn*, and subjected to transwell and wound healing assays. Scale bar, 100 μm. Data represent mean ± SEM. *$p < 0.05$, **$p < 0.01$, ***$p < 0.001$.

miR-122-5p expression. Furthermore, exosomal miR-122-5p shows promise as a noninvasive biomarker for predicting CRC metastasis. Inhibiting the excretion of miR-122-5p could be a promising therapeutic approach to mitigate the detrimental effects of *Fn* infection. Moreover, exosomal miR-122-5p might be a noninvasive biomarker for prediction of CRC metastasis. The current study expands upon existing knowledge regarding the role of *Fn* in the development of CRC.

In recent years, studies have focused on the role of exosomal miRNAs derived from human cells infected with various pathogens.[21,26] Distinct from previous reports, this study screened for the first time the exosomal miRNAs in CRC patients infected with distinct abundance of *Fn*. Notably, miR-122-5p was upregulated only in the serum of CRC patients but was downregulated in matched tumor tissues. Moreover, *in vitro* and *in vivo* experiments illustrated that miR-122-5p functioned as a tumor suppressor in *Fn*-infected CRC cells. These findings are similar to some previous reports regarding the activity of miR-122-5p in CRC.[27,28] Thus, we hypothesize that *Fn* promotes CRC progression by downregulating the expression of intracellular miR-122-5p. Previous studies have reported that miR-122-5p is detectable in the serum/plasma exosomes of cancer patients.[29,30] The present study revealed that exosomal miR-122-5p was increased in the serum of *Fn*-infected CRC patients. Moreover, the levels of exosomal miR-122-5p were enhanced in patients with lymph node metastasis or distal metastasis status. Our previous meta-analysis revealed that *Fn* was more abundant in CRC patients with metastasis.[11] Therefore, considering these data, it is likely that *Fn* promotes metastasis through the downregulation of intracellular miR-122-5p. And intracellular miR-122-5p might be into exosomes, then sumoylated hnRNPA2B1 might be involved in the sorting of miR-122-5p into exosomes.[31] Inhibiting the excretion of miR-122-5p could be a promising therapeutic approach to mitigate the detrimental effects of *Fn* infection.

It is well known that miRNAs exert their effects by inhibiting downstream target genes. To search for the targets of miR-122-5p in *Fn*-infected CRC cells, we reanalyzed our RNA-seq data deposited in the Sequence Read Archive (No. PRJNA777960). Among the potential interacting genes, FUT8 emerged as a possible central target. FUT8 encodes an enzyme belonging to the family of fucosyltransferases and is the only fucosyltransferase involved in core fucosylation.[32] It has been reported that FUT8 is overexpressed in multiple cancers and contributes to the malignancy of tumor cells.[33–36] However, its role in *Fn*-associated CRC development is unclear. The present study illustrates that *Fn* infection enhanced FUT8 expression by reducing the expression of miR-122-5p. Moreover, FUT8 overexpression reversed the hindrance that miR-122-5p exerts upon migration and invasion in CRC cells, and knockdown of FUT8 precluded *Fn*-induced metastasis *in vitro* and *in vivo*. In contrast, miR-122-5p overexpression augmented FUT8 expression in *Fn*-treated CRC cells, yet similar trends were not observed in CRC cells without *Fn* infection, probably owing to their high levels of suppressive miR-122-5p expression. Therefore, for the first time, we established inverse linkages between miR-122-5p and FUT8 in CRC cells treated with *Fn*.

Our previous study revealed that *Fn* could induce EMT in tumor cells, yet the molecular mechanisms driving this are still unclear.[37] Meanwhile, some research has reported that FUT8 activates EMT in several cancers.[35,38] As hypothesized, our studies indicated that restraining miR-122-5p promoted EMT by activating FUT8 in *Fn*-infected CRC cells, a phenomenon that could be attenuated by knockdown of FUT8. Conversely, elevated levels of miR-122-5p hindered EMT and could be compromised by re-expression of FUT8. Similarly, Ding et al. reported that miR-122-5p negatively mediates the TGF-β1/Smads signaling pathway in skeletal muscle myogenesis, supporting our findings from an additional perspective.[39] TGF-β1 is considered as a major EMT inducer, and as such, accumulating evidence has suggested that TGF-β1-induced EMT strongly influences cancer progression and metastasis, in particular by activation and transcriptional regulation of Smad or non-Smad pathway signaling.[40] Further evidences have demonstrated that there is a positive feedback loop of FUT8/TGF-β1 that regulates EMT and tumor progression.[38,41] Consistent with these previous reports, our study also illustrated that TGF-β1 induced clear EMT accompanied by upregulation of FUT8; this enhanced FUT8 expression could be weakened by overexpression of miR-122-5p, highlighting that miR-122-5p is a vital mediator in *Fn*-induced EMT. Correspondingly, a positive correlation was observed between the expression of TGF-β1 and FUT8 in CRC tissue.

In the study presented herein, we further revealed that the TGF-β1/Smads signaling pathway is a major target of the miR-122-5p regulation network that interacts via FUT8 to facilitate CRC cells with an invasive phenotype. MiR-122-5p overexpression exerts its repressive activity on TGF-β1/Smads signaling, reducing Smad2/3 phosphorylation, effects that are reversed by reintroduction of FUT8. Given that SB431542 was able to inactivate EMT and block FUT8 expression in miR-122-5p inhibition groups, it was verified that the TGF-β1/Smads signaling is essential for miR-122-5p/FUT8-induced EMT function. Overall, our data support that decreased miR-122-5p expression induced by *Fn* infection promotes CRC metastasis by facilitating TGF-β1/Smads-mediated EMT. Thus, it may be possible to alleviate EMT by antagonizing the TGF-β1/Smads pathway to prevent CRC metastasis, revealing a potential therapeutic target for CRC.

In summary, we elucidated that *Fn* infection promoted CRC malignancy by accelerating the excretion of exosome-wrapped miR-122-5p. Furthermore, the miR-122-5p/FUT8/TGF-β1/Smads axis exerted a critical role during *Fn*-induced metastasis in CRC, revealing a potential

mechanism by which *Fn*-induced miRNAs promote intestinal metastasis. Our studies open avenues for targeting microbiota and miRNAs to prevent intestinal metastasis.

Limitations of the study

There are some limitations that merit consideration. As we known, a single miRNA is not expected to have a major impact on cancer progression. In addition to miR-122-5p, the other miRNAs differentially expressed between *Fn*-positive and *Fn*-negative patients might also impact on CRC cells. In the current study, we also did not study what effect exosomal miR-122-5p induced by *Fn* infection on other cells within a tumor microenvironment. And, it is unclear which product of *Fn* is responsible for this effect.

STAR★METHODS

Detailed methods are provided in the online version of this paper and include the following:

- KEY RESOURCES TABLE
- RESOURCE AVAILABILITY
  - Lead contact
  - Materials availability
  - Data and code availability
- EXPERIMENTAL MODEL AND SUBJECT DETAILS
  - Clinical specimens
  - Bacterial strains and culture conditions
  - Cell lines and cell culture
  - Xenograft models
- METHOD DETAILS
  - *Fn* DNA detection
  - Exosomes isolation and identification
  - RNA extraction and RT-qPCR
  - Western blotting analysis
  - Cell migration and invasion assay
  - Cell infection with *Fn* experiment
  - Fluorescence *in situ* hybridization (FISH)
  - Dual-luciferase reporter assay
  - RNA pull down
  - RNA immunoprecipitation
  - Immunohistochemistry (IHC)
- QUANTIFICATION AND STATISTICAL ANALYSIS

SUPPLEMENTAL INFORMATION

Supplemental information can be found online at https://doi.org/10.1016/j.isci.2023.107686.

ACKNOWLEDGMENTS

The work was supported by Natural Science Foundation of Shandong Province under Grant ZR2021MH110; ZR2020MH238; ZR2020MH257, and National Natural Science Foundation of China under Grant 82172339; 81972005, and Taishan scholar program of Shandong Province.

AUTHOR CONTRIBUTIONS

Yi Z. and X.Z. conceived and designed the study. M.Z., Y.F.W., Y.Z., and Y.L.W. conducted the experiments. Z.S., Y.X., X.L., L.Y., and N.N.N. contributed to the data analysis. M.Z., Y.F.W., and X.Z. wrote and revised the manuscript. Yi Z. and X.Z. supervised the research. All authors read and approved the final manuscript.

DECLARATION OF INTERESTS

The authors declare no competing interests.

Received: March 22, 2023
Revised: July 23, 2023
Accepted: August 17, 2023
Published: August 19, 2023

REFERENCES

1. Sung, H., Ferlay, J., Siegel, R.L., Laversanne, M., Soerjomataram, I., Jemal, A., and Bray, F. (2021). Global Cancer Statistics 2020: GLOBOCAN Estimates of Incidence and Mortality Worldwide for 36 Cancers in 185 Countries. CA. Cancer J. Clin. *71*, 209–249. https://doi.org/10.3322/caac.21660.
2. Al Bandar, M.H., and Kim, N.K. (2017). Current status and future perspectives on treatment of liver metastasis in colorectal cancer (Review). Oncol. Rep. *37*, 2553–2564. https://doi.org/10.3892/or.2017.5531.
3. Bird, N.C., Mangnall, D., and Majeed, A.W. (2006). Biology of colorectal liver metastases: A review. J. Surg. Oncol. *94*, 68–80. https://doi.org/10.1002/jso.20558.
4. Beckers, R.C.J., Lambregts, D.M.J., Lahaye, M.J., Rao, S.-X., Kleinen, K., Grootscholten, C., Beets, G.L., Beets-Tan, R.G.H., and Maas, M. (2018). Advanced imaging to predict response to chemotherapy in colorectal liver metastases - a systematic review. HPB (Oxford) *20*, 120–127. https://doi.org/10.1016/j.hpb.2017.10.013.
5. Coker, O.O., Liu, C., Wu, W.K.K., Wong, S.H., Jia, W., Sung, J.J.Y., and Yu, J. (2022). Altered gut metabolites and microbiota interactions are implicated in colorectal carcinogenesis and can be non-invasive diagnostic biomarkers. Microbiome *10*, 35. https://doi.org/10.1186/s40168-021-01208-5.
6. Janney, A., Powrie, F., and Mann, E.H. (2020). Host–microbiota maladaptation in colorectal cancer. Nature *585*, 509–517. https://doi.org/10.1038/s41586-020-2729-3.
7. Brennan, C.A., and Garrett, W.S. (2019). Fusobacterium nucleatum — symbiont, opportunist and oncobacterium. Nat. Rev. Microbiol. *17*, 156–166. https://doi.org/10.1038/s41579-018-0129-6.
8. Kostic, A.D., Chun, E., Robertson, L., Glickman, J.N., Gallini, C.A., Michaud, M., Clancy, T.E., Chung, D.C., Lochhead, P., Hold, G.L., et al. (2013). Fusobacterium nucleatum Potentiates Intestinal Tumorigenesis and Modulates the Tumor-Immune Microenvironment. Cell Host Microbe *14*, 207–215. https://doi.org/10.1016/j.chom.2013.07.007.
9. Rubinstein, M.R., Wang, X., Liu, W., Hao, Y., Cai, G., and Han, Y.W. (2013). Fusobacterium nucleatum Promotes Colorectal Carcinogenesis by Modulating E-Cadherin/β-Catenin Signaling via its FadA Adhesin. Cell Host Microbe *14*, 195–206. https://doi.org/10.1016/j.chom.2013.07.012.
10. Bullman, S., Pedamallu, C.S., Sicinska, E., Clancy, T.E., Zhang, X., Cai, D., Neuberg, D., Huang, K., Guevara, F., Nelson, T., et al. (2017). Analysis of Fusobacterium persistence and antibiotic response in colorectal cancer. Science *358*, 1443–1448. https://doi.org/10.1126/science.aal5240.
11. Chen, W.D., Zhang, X., Zhang, Y.P., Yue, C.B., Wang, Y.L., Pan, H.W., Zhang, Y.L., Liu, H., and Zhang, Y. (2022). Fusobacterium Nucleatum Is a Risk Factor for Metastatic Colorectal Cancer. Curr. Med. Sci. *42*, 538–547. https://doi.org/10.1007/s11596-022-2597-1.
12. Yang, Y., Weng, W., Peng, J., Hong, L., Yang, L., Toiyama, Y., Gao, R., Liu, M., Yin, M., Pan, C., et al. (2017). Fusobacterium nucleatum Increases Proliferation of Colorectal Cancer Cells and Tumor Development in Mice by Activating Toll-Like Receptor 4 Signaling to Nuclear Factor−κB, and Up-regulating Expression of MicroRNA-21. Gastroenterology *152*, 851–866.e24. https://doi.org/10.1053/j.gastro.2016.11.018.
13. Lu, X., Xu, Q., Tong, Y., Zhang, Z., Dun, G., Feng, Y., Tang, J., Han, D., Mao, Y., Deng, L., et al. (2022). Long non-coding RNA EVADR induced by Fusobacterium nucleatum infection promotes colorectal cancer metastasis. Cell Rep. *40*, 111127. https://doi.org/10.1016/j.celrep.2022.111127.
14. Chen, S., Su, T., Zhang, Y., Lee, A., He, J., Ge, Q., Wang, L., Si, J., Zhuo, W., and Wang, L. (2020). Fusobacterium nucleatum promotes colorectal cancer metastasis by modulating KRT7-AS/KRT7. Gut Microb. *11*, 511–525. https://doi.org/10.1080/19490976.2019.1695494.
15. Wang, B., Wang, H., and Yang, Z. (2012). MiR-122 Inhibits Cell Proliferation and Tumorigenesis of Breast Cancer by Targeting IGF1R. PLoS One *7*, e47053. https://doi.org/10.1371/journal.pone.0047053.
16. Gao, Z., Wang, Q., Ji, M., Guo, X., Li, L., and Su, X. (2021). Exosomal lncRNA UCA1 modulates cervical cancer stem cell self-renewal and differentiation through microRNA-122-5p/SOX2 axis. J. Transl. Med. *19*, 229. https://doi.org/10.1186/s12967-021-02872-9.
17. Wu, Q., He, Y., Liu, X., Luo, F., Jiang, Y., Xiang, M., and Zhao, R. (2023). Cancer stem cell-like cells-derived exosomal lncRNA CDKN2B-AS1 promotes biological characteristics in thyroid cancer via miR-122-5p/P4HA1 axis. Regen. Ther. *22*, 19–29. https://doi.org/10.1016/j.reth.2022.11.005.
18. Yang, X., Sun, L., Wang, L., Yao, B., Mo, H., and Yang, W. (2019). LncRNA SNHG7 accelerates the proliferation, migration and invasion of hepatocellular carcinoma cells via regulating miR-122-5p and RPL4. Biomed. Pharmacother. *118*, 109386. https://doi.org/10.1016/j.biopha.2019.109386.
19. Chen, F., Li, Y., Aye, L., Wu, Y., Dong, L., Yang, Z., Gao, Q., and Zhang, S. (2023). FUT8 is regulated by miR-122-5p and promotes malignancies in intrahepatic cholangiocarcinoma via PI3K/AKT signaling. Cell. Oncol. *46*, 79–91. https://doi.org/10.1007/s13402-022-00736-y.
20. Kalluri, R. (2016). The biology and function of exosomes in cancer. J. Clin. Invest. *126*, 1208–1215. https://doi.org/10.1172/JCI81135.
21. Guo, S., Chen, J., Chen, F., Zeng, Q., Liu, W.-L., and Zhang, G. (2020). Exosomes derived from Fusobacterium nucleatum-infected colorectal cancer cells facilitate tumour metastasis by selectively carrying miR-1246/92b-3p/27a-3p and CXCL16. Gut *70*, 1507–1519. https://doi.org/10.1136/gutjnl-2020-321187.
22. Chen, C., Yu, H., Han, F., Lai, X., Ye, K., Lei, S., Mai, M., Lai, M., and Zhang, H. (2022). Tumor-suppressive circRHOBTB3 is excreted out of cells via exosome to sustain colorectal cancer cell fitness. Mol. Cancer *21*, 46. https://doi.org/10.1186/s12943-022-01511-1.
23. Cook, K.B., Kazan, H., Zuberi, K., Morris, Q., and Hughes, T.R. (2011). RBPDB: a database of RNA-binding specificities. Nucleic Acids Res. *39*, D301–D308. https://doi.org/10.1093/nar/gkq1069.
24. Massagué, J. (2008). TGFβ in Cancer. Cell *134*, 215–230. https://doi.org/10.1016/j.cell.2008.07.001.
25. Wei, S., Zhang, J., Wu, X., Chen, M., Huang, H., Zeng, S., Xiang, Z., Li, X., and Dong, W. (2023). Fusobacterium nucleatum Extracellular Vesicles Promote Experimental Colitis by Modulating Autophagy via the miR-574-5p/CARD3 Axis. Inflamm. Bowel Dis. *29*, 9–26. izac177. https://doi.org/10.1093/ibd/izac177.
26. Cao, Y., Wang, Z., Yan, Y., Ji, L., He, J., Xuan, B., Shen, C., Ma, Y., Jiang, S., Ma, D., et al. (2021). Enterotoxigenic Bacteroides fragilis Promotes Intestinal Inflammation and Malignancy by Inhibiting Exosome-Packaged miR-149-3p. Gastroenterology *161*, 1552–1566.e12. https://doi.org/10.1053/j.gastro.2021.08.003.
27. Shen, Q., Wang, R., Liu, X., Song, P., Zheng, M., Ren, X., Ma, J., Lu, Z., and Li, J. (2022). HSF1 Stimulates Glutamine Transport by Super-Enhancer-Driven lncRNA LINC00857 in Colorectal Cancer. Cancers *14*, 3855. https://doi.org/10.3390/cancers14163855.
28. Yin, W., Xu, J., Li, C., Dai, X., Wu, T., and Wen, J. (2020). Circular RNA circ_0007142 Facilitates Colorectal Cancer Progression by Modulating CDC25A Expression via miR-122-5p. Onco Targets Ther. *13*, 3689–3701. https://doi.org/10.2147/OTT.S238338.
29. Marin, A.M., Mattar, S.B., Amatuzzi, R.F., Chammas, R., Uno, M., Zanette, D.L., and Aoki, M.N. (2022). Plasma Exosome-Derived microRNAs as Potential Diagnostic and Prognostic Biomarkers in Brazilian Pancreatic Cancer Patients. Biomolecules *12*, 769. https://doi.org/10.3390/biom12060769.
30. Chen, J., Wu, W., He, X., Jia, L., Yang, J., Si, X., Yu, K., Li, S., Qiu, Y., Xu, K., et al. (2021). Exosomal miR-122-5p is Related to the Degree of Myelosuppression Caused by Chemotherapy in Patients with Colorectal Cancer. Cancer Manag. Res. *13*, 8329–8339. https://doi.org/10.2147/CMAR.S332384.
31. Villarroya-Beltri, C., Gutiérrez-Vázquez, C., Sánchez-Cabo, F., Pérez-Hernández, D., Vázquez, J., Martin-Cofreces, N., Martinez-Herrera, D.J., Pascual-Montano, A., Mittelbrunn, M., and Sánchez-Madrid, F. (2013). Sumoylated hnRNPA2B1 controls the sorting of miRNAs into exosomes through binding to specific motifs. Nat. Commun. *4*, 2980. https://doi.org/10.1038/ncomms3980.
32. Bastian, K., Scott, E., Elliott, D.J., and Munkley, J. (2021). FUT8 Alpha-(1,6)-Fucosyltransferase in Cancer. Int. J. Mol. Sci. *22*, 455. https://doi.org/10.3390/ijms22010455.
33. Li, C., Xin, Z., He, L., Ning, J., Lin, K., Pan, J., Rao, J., Wang, G., and Zhu, H. (2021). cFUT8 promotes liver cancer progression by miR-548c/FUT8 axis. Sig. Transduct. Target Ther. *6*, 30–33. https://doi.org/10.1038/s41392-020-00393-3.
34. Li, F., Zhao, S., Cui, Y., Guo, T., Qiang, J., Xie, Q., Yu, W., Guo, W., Deng, W., Gu, C., and Wu, T. (2020). α1,6-Fucosyltransferase (FUT8) regulates the cancer-promoting capacity of cancer-associated fibroblasts (CAFs) by modifying EGFR core fucosylation (CF) in non-small cell lung cancer (NSCLC). Am. J. Cancer Res. *10*, 816–837.
35. Tu, C.-F., Wu, M.-Y., Lin, Y.-C., Kannagi, R., and Yang, R.-B. (2017). FUT8 promotes breast cancer cell invasiveness by remodeling TGF-β receptor core fucosylation. Breast Cancer Res. *19*, 111. https://doi.org/10.1186/s13058-017-0904-8.

36. Lin, S., Zhou, L., Dong, Y., Yang, Q., Yang, Q., Jin, H., Yuan, T., and Zhou, S. (2021). Alpha-(1,6)-fucosyltransferase (FUT8) affects the survival strategy of osteosarcoma by remodeling TNF/NF-κB2 signaling. Cell Death Dis. *12*, 1124. https://doi.org/10.1038/s41419-021-04416-x.

37. Chen, W.-D., Zhang, X., Zhang, M.-J., Zhang, Y.-P., Shang, Z.-Q., Xin, Y.-W., and Zhang, Y. (2022). Salivary Fusobacterium nucleatum serves as a potential diagnostic biomarker for gastric cancer. World J. Gastroenterol. *28*, 4120–4132. https://doi.org/10.3748/wjg.v28.i30.4120.

38. Chen, C.-Y., Jan, Y.-H., Juan, Y.-H., Yang, C.-J., Huang, M.-S., Yu, C.-J., Yang, P.-C., Hsiao, M., Hsu, T.-L., and Wong, C.-H. (2013). Fucosyltransferase 8 as a functional regulator of nonsmall cell lung cancer. Proc. Natl. Acad. Sci. USA *110*, 630–635. https://doi.org/10.1073/pnas.1220425110.

39. Sun, Y., Wang, H., Li, Y., Liu, S., Chen, J., and Ying, H. (2018). miR-24 and miR-122 Negatively Regulate the Transforming Growth Factor-β/Smad Signaling Pathway in Skeletal Muscle Fibrosis. Mol. Ther. Nucleic Acids *11*, 528–537. https://doi.org/10.1016/j.omtn.2018.04.005.

40. Hata, A., and Chen, Y.-G. (2016). TGF-β Signaling from Receptors to Smads. Cold Spring Harb. Perspect. Biol. *8*, a022061. https://doi.org/10.1101/cshperspect.a022061.

41. Lin, H., Wang, D., Wu, T., Dong, C., Shen, N., Sun, Y., Sun, Y., Xie, H., Wang, N., and Shan, L. (2011). Blocking core fucosylation of TGF-β1 receptors downregulates their functions and attenuates the epithelial-mesenchymal transition of renal tubular cells. Am. J. Physiol. Renal Physiol. *300*, F1017–F1025. https://doi.org/10.1152/ajprenal.00426.2010.

STAR★METHODS

KEY RESOURCES TABLE

REAGENT or RESOURCE	SOURCE	IDENTIFIER
Antibodies		
Anti-FUT8	Abcam	Cat#191571; RRID: AB_2800511
Anti-Alix	Abcam	Cat#275377
Anti-CD63	Abcam	Cat#134045; RRID: AB_2800495
Anti-Calnexin	Abcam	Cat#22595; RRID: AB_2069006
Anti-Vimentin	CST	Cat#5741; RRID: AB_10695459
Anti-Snail	CST	Cat#3879; RRID: AB_2255011
Anti-Slug	CST	Cat#9585; RRID: AB_2239535
Anti-N-Cadherin	CST	Cat#13116; RRID: AB_2687616
Anti-E-Cadherin	CST	Cat#3195; RRID: AB_2291471
Anti-hnRNPA2B1	Abcam	Cat#259894
Anti-Smad2	Abcam	Cat#ab40855; RRID: AB_777977
Anti-Smad3	Abcam	Cat#ab40854; RRID: AB_777979
Anti-P-smad2	Abcam	Cat#ab30079
Anti-P-smad3	Abcam	Cat#40854; RRID: AB_777979
Anti-GAPDH	CST	Cat#5174; RRID: AB_10622025
Anti-Rabbit IgG	CST	Cat#7074; RRID: AB_2099233
Bacterial and virus strains		
Fusobacterium nucleatum	ATCC	ATCC 49256
Fusobacterium nucleatum	ATCC	ATCC 25586
Escherichia coli	Tiangen	BMZ135405
Biological samples		
Colonic patient samples (serum and tumor tissue)	Qilu Hospital of Shandong University	N/A
Chemicals, peptides, and recombinant proteins		
Wilkins chalgren broth	Sigma	CM0643
Columbia agar plates	Oxoid, UK	CM0331
Metronidazole	Sigma	Cat# M1547
TRIzol	Invitrogen	Cat# 15596026
Fetal bovine serum	Gibco	Cat# 10100147
DAPI	Sigma	Cat# D9642
4% paraformaldehyde	Beyotime	Cat# P0099
PMSF	Beyotime	Cat# ST506
DMEM	Gibco	C11965500BT
PBS	Gibco	70011044
Triton X-100	Sigma-aldrich	Cat# SLBT3016
TWEEN	J.T.Baker X251-07	CAS 9005-64-5
BSA	Sigma-Aldrich A7906	CAS 9048-46-8
Lipofectamine 3000	Invitrogen	Cat# L3000015
riboFECT CP Transfection Kit	Ribobio	C10511-05
Critical commercial assays		
QIAamp DNA Mini Kit	Qiagen	Cat# 51304

(*Continued on next page*)

Continued

REAGENT or RESOURCE	SOURCE	IDENTIFIER
miRNA 1st Strand cDNA Synthesis Kit	Vazyme	MR101-01
HiScript II 1st Strand cDNA Synthesis Kit	Vazyme	R211-01
ChamQ SYBR qPCR Master Mix	Vazyme	Q311-02
BCA assay	Thermo Scientific	A53225
QIAGEN DNeasy Blood and Tissue Kit	Qiagen	69504
2×AceQ qPCR Probe Master Mix	Vazyme	Q112-02
Experimental models: Cell lines		
LoVo cells	ATCC	ATCC CCL-229
SW480 cells	ATCC	ATCC CCL-228
SW620 cells	ATCC	ATCC CCL-227
HT29 cells	ATCC	ATCC HTB-38
HCT116 cells	ATCC	ATCC CBP-60028
Experimental models: Organisms/strains		
BALB/c mice	Beijing Speffer	B201-02
Oligonucleotides		
See Table S4 for oligonucleotide information	This paper	N/A
Software and algorithms		
GraphPad Prism, 9.1	GraphPad Software	https://www.graphpad.com
SPSS Statistics 20.0 software	IBM	https://www.ibm.com/spss

RESOURCE AVAILABILITY

Lead contact

Further information and requests for resources and reagents should be directed to and will be fulfilled by the lead contact, Xin Zhang (xinzhang@sdu.edu.cn).

Materials availability

Plasmids generated in this study are available from the lead contact.

Data and code availability

- All data reported in this paper will be shared by the lead contact upon request.
- This paper does not report original code.
- Any additional information required to reanalyze the data reported in this paper is available from the lead contact upon request.

EXPERIMENTAL MODEL AND SUBJECT DETAILS

Clinical specimens

All subjects were enrolled from Qilu Hospital of Shandong University and provided informed consent. This study was approved by the ethics committee of Qilu Hospital of Shandong University.

Bacterial strains and culture conditions

Fn strains (ATCC49256 and ATCC25586) were purchased from the American Type Culture Collection (ATCC, USA) and cultured in Anaerobe Basal Broth plates under anaerobic conditions at 37°C. Escherichia coli (DH5α, Tiangen, China) was cultured aerobically in LB agar plates at 37°C.

Cell lines and cell culture

CRC cell lines (LOVO, HT-29, SW620, SW480, and HCT116) were purchased from American Type Culture Collection (ATCC). HCT116 cells and SW480 cells were maintained in Dulbecco's modified Eagle's medium (DMEM) (Gibco, Austria) supplemented with 10% fetal bovine serum (Gibco, Austria) and 1% penicillin/streptomycin (Solarbio, China). LOVO and HT-29 cells were maintained in RPMI 1640 (Gibco, Austria)

supplemented with 10% fetal bovine serum (Gibco, Austria) and 1% penicillin/streptomycin (Solarbio, China). Cell culture was maintained at 37°C and 5% CO_2. We test the cells for mycoplasma on a regular basis.

Xenograft models

BALB/c athymic nude mice (4–5 weeks old) were chosen to quantify the metastatic process *in vivo*, 3×10^6 HCT116 cells that had been treated with *Fn* or transfected with lentiviral vectors were injected into the spleens of the mice. All animal studies were approved by the Animal Care and Use Committee of Qilu Hospital of Shandong University.

METHOD DETAILS

Fn DNA detection

DNA was extracted from CRC tissues using the QIAGEN DNeasy Blood and Tissue Kit (Qiagen, Hilden, Germany), and amplified using 2× AceQ qPCR Probe Master Mix (Vazyme, Nanjing, China). The level of *Fn* DNA was calculated using the $2^{-\Delta Ct}$ method, in which ΔCt refers to the difference in Ct values between nusG gene of *Fn* and human reference gene SLCO2A1.

Exosomes isolation and identification

To obtain CRC cell-derived exosomes, SW480 and HCT116 cell lines were cultured in exosome-free medium. The conditioned medium was collected and centrifuged at 4 °C at 300 g for 10 min, 2,000 g for 10 min, and 10,000 g for 30 min to remove residual cells and debris. For serum exosomes isolation, the 500 μL serum was centrifuged at 2,000g for 30 min, and centrifuged at 10,000g for 30 min. Then, the supernatants come from cell cultures or sera were further filtered through a 0.22 μm filter (Millipore, USA). Finally, the filtrates were ultracentrifuged twice at 100,000 g for 90 min (Beckman Coulter, USA) to collect the pellet, which was finally resuspended in ice-cold PBS. The morphology of the extracted exosomes was observed using transmission electron microscopy (JEM-1-11 microscope, Japan). The nanoparticle size of the exosomes was analyzed using a nanoparticle tracking system ZetaView PMX 110 (Particle Metrix, Germany), and signature exosome proteins, including TSG101, CD63 and Alix, were identified by western blotting.

RNA extraction and RT-qPCR

TRIzol or TRIzol LS reagent (Invitrogen, USA) was used to extract total RNA from tissues or exosomes according to the manufacturer's instruction. MiRNAs or mRNA reverse transcription was performed using miRNA 1st Strand cDNA Synthesis Kit or HiScript II 1st Strand cDNA Synthesis Kit (Vazyme, China) respectively, and qPCR was carried out using ChamQ SYBR qPCR Master Mix (Vazyme, China) in QuantStudio 5 Real-Time PCR system (Applied Biosystems, Denmark). The relative expression level of targets was computed using the comparative Ct method through normalized to reference genes GAPDH mRNA and U6 snRNA, respectively. The sequences of all primers are listed in Table S4.

Western blotting analysis

Total cellular protein was extracted from tissue samples with RIPA lysis and extraction buffer (Thermo Scientific, USA) before total protein content was determined using the BCA assay (Thermo Scientific, USA). Protein samples of equal content were run on a 10% SDS-PAGE gel and transferred to PVDF membranes prior to blocking with 5% nonfat milk and incubation overnight at 4°C with the primary antibodies. The membranes were then incubated with the appropriate secondary antibodies for 1 h at room temperature. The results were quantified by densitometry using Amersham ImageQuant 800 (Cytiva, USA).

Cell migration and invasion assay

For the migration experiment, CRC cells in serum-free medium (200 μL) were seeded in the upper well of a Corning Transwell insert chamber (8.0 μm pore size). The corresponding CM (600 μL) was added to the lower chambers. After incubating at 37°C for 24 h, the transmembrane was fixed with 4% paraformaldehyde for 15–20 min before being stained with crystal violet for 15 min. Finally, the number of migrated cells was counted using an inverted optical microscope (Olympus, Japan) in five randomly selected fields. Each experiment was repeated in triplicate. For the invasion assay, the upper chamber was coated with Matrigel (BD Biosciences, USA) before inoculation and the remaining process was identical to the migration assay.

Cell infection with *Fn* experiment

CRC cells were seeded into 6-well plates at 5 × 105/well and infected with Fn for 2 h. Next, cells were washed with PBS twice and cultured in complete medium supplied with 0.01 μg/mL metronidazole for different experimental objects.

Fluorescence *in situ* hybridization (FISH)

FISH assays were conducted using the fluorescent *in situ* hybridization Kit (RiboBio, China) according to the manufacturer's instructions. Cy3-labeled miR-122-5p probes were synthesized by Ribo-Bio (RiboBio, China). 3×10^4 cells grew on the glass slide of 24-well plate and cell confluency reached 60%–70%. Then, PBS washed cells and fixed with 4% formaldehyde. Next, PBS washed cells and added precooled 0.2% Triton

X-100 at 4 °C. Following discarding the above solution, PBS washed cells. Prehybridization solution were added to block at 37 °C and discarded. Then probe hybridization solution were applied to incubate with cells at 37 °C overnight in the dark. Following washing with hybridization buffer, 4′,6-diamidino-2-phenylindole (DAPI) was used to stain the nuclei. Finally, PBS washed cells for 5 min, 3 times.

Dual-luciferase reporter assay

CRC cells were cotransfected with wild-type or mutant luciferase plasmids and the firefly luciferase reporter vector in the presence of miR-122-5p mimics/inhibitors/respective NC. After 48 h, the Dual-Luciferase Assay Kit (Vazyme, China) was used to quantify luciferase activity according to the manufacturer's protocol. Firstly, cell Lysis Buffer was applied to lysis treated cells for 5 min and centrifuged at 12,000g for 2 min at room temperature. Following quickly mixed Luciferase Substrate and cell lysis supernatant, Firefly luciferase reporter gene activity was detected in microplate reader. Next, added Renilla subtract working solution into the above reaction solution, and then immediately detected the Renilla luciferase reporter gene activity in microplate reader.

RNA pull down

The biotin-labeled miR-122-5p probes were generated by RiboBio (RiboBio, China). CRC cells were transfected with biotin-labeled wild-type and mutant miR-122-5p, and we collected cytoplasmic, nuclear and exosomal extracts. Then, above extracts were incubated with biotin labeled wild-type and mutant miR-122-5p probes to form RNA-protein complexes. Next, the above complexes were incubated with anti-hnRNPA2B1 or anti-IgG coated magnetic beads (Invitrogen, USA) at 4°C overnight; After elution, RNA-binding proteins were eluted and detected by western blotting using anti-hnRNPA2B1 (#259894, Abcam, UK).

RNA immunoprecipitation

RNA immunoprecipitation (RIP) assays were conducted using the RNA Immunoprecipitation Kit (Geneseed, China) according to the manufacturer's instructions. CRC cells and CRC cell-derived exosomes were harvested, lysed using lysis buffer A and centrifuged at 14,000 g at 4 °C for 10 min. Then, IgG antibody (Millipore, USA) and hnRNPA2B1 antibody (#259894, Abcam, UK) were incubated with blocked beads and discarded the supernatant. Cell lysis supernatant was mixed with beads coated with anti-hnRNPA2B1 or anti-IgG 4°C, 10r/min rotating reaction overnight. Next, unbound substances were removed by washing with buffer 5–10 times. Finally, immunoprecipitated RNA was extracted and purified using centrifuge columns and assayed using RT-qPCR.

Immunohistochemistry (IHC)

Tissue tissues from CRC patients were first fixed in 4% paraformaldehyde and embedded in paraffin. Sections were blocked with 10% goat serum and incubated with the FUT8 antibody at 4°C overnight. Then, the sections were incubated with HRP-conjugated goat anti-rabbit secondary antibody for 1 h at room temperature. A DAB kit (Solarbio, China) was used to detect activities, and hematoxylin was applied to stain the slides.

QUANTIFICATION AND STATISTICAL ANALYSIS

Statistical analyses were performed using GraphPad Prism Software (GraphPad Software, USA) and SPSS Software (SPSS Software, USA). Student's *t* test, one-way ANOVA, Mann Whitney test or Spearman correlation was applied to analyze. All experiments were carried out in replicates of three, and the data are presented as mean ± SD. $p < 0.05$ was considered statistically significant.